# Cellular Sensing Governs the Stability of Chemotactic Fronts

Ricard Alert,[1,2,3,4,*] Alejandro Martínez-Calvo,[1,5] and Sujit S. Datta[5,†]
[1]Princeton Center for Theoretical Science, Princeton University, Princeton, New Jersey 08544, USA
[2]Lewis-Sigler Institute for Integrative Genomics, Princeton University, Princeton, New Jersey 08544, USA
[3]Max Planck Institute for the Physics of Complex Systems, Nöthnitzerstraße 38, 01187 Dresden, Germany
[4]Center for Systems Biology Dresden, Pfotenhauerstraße 108, 01307 Dresden, Germany
[5]Department of Chemical and Biological Engineering, Princeton University, Princeton, New Jersey 08544, USA

(Received 24 July 2021; accepted 28 February 2022; published 8 April 2022)

In contexts ranging from embryonic development to bacterial ecology, cell populations migrate chemotactically along self-generated chemical gradients, often forming a propagating front. Here, we theoretically show that the stability of such chemotactic fronts to morphological perturbations is determined by limitations in the ability of individual cells to sense and thereby respond to the chemical gradient. Specifically, cells at bulging parts of a front are exposed to a smaller gradient, which slows them down and promotes stability, but they also respond more strongly to the gradient, which speeds them up and promotes instability. We predict that this competition leads to chemotactic fingering when sensing is limited at too low chemical concentrations. Guided by this finding and by experimental data on *E. coli* chemotaxis, we suggest that the cells' sensory machinery might have evolved to avoid these limitations and ensure stable front propagation. Finally, as sensing of any stimuli is necessarily limited in living and active matter in general, the principle of sensing-induced stability may operate in other types of directed migration such as durotaxis, electrotaxis, and phototaxis.

DOI: 10.1103/PhysRevLett.128.148101

Fronts are propagating interfaces that allow one spatial domain to invade another. They are ubiquitous in nature, arising for example during phase transitions, autocatalytic chemical reactions, and flame propagation [1–6]. Biology also abounds with examples, such as fronts of gene expression during development, electric signals in the heart and the brain, infection during disease outbreaks, and expanding populations in ecosystems [7–9]. These examples can all be modeled as reaction-diffusion systems (e.g., using the Fisher-KPP equation [10,11]), for which both the motion and morphologies of fronts are well understood [1–6].

Another prominent and separate class of fronts is that of *chemotactic fronts*, in which active agents collectively migrate in response to a self-generated chemical gradient. These fronts have long been observed in bacterial populations, enabling cells to escape from harmful conditions, colonize new terrain, and coexist [12–21]. More generally, collective chemotaxis plays crucial roles in slime mold aggregation [22], embryonic development [23–25], immune response [26], and cancer progression [27,28]. Beyond cell populations, enzymes [29–31] and synthetic active colloids [32–34] also exhibit collective chemotaxis. Therefore, studies of chemotactic fronts are of broad interest in biological and active matter physics. However, while the motion of chemotactic fronts can be successfully modeled in certain cases [17,18,20,21,35–39], a general understanding of how their morphologies evolve—akin to that of reaction-diffusion systems—remains lacking.

For example, a fundamental feature of a front is its morphological stability: Do shape perturbations decay or grow over time? This question is well-studied in nonliving systems. In many cases, flat fronts are unstable, leading to striking dendritic patterns at fluid and solid interfaces as in the case of the well-studied Saffman-Taylor and Mullins-Sekerka instabilities [6,40–46]. In active and living matter, front instabilities underlie fingering patterns in active colloids [47], growing tumors [48,49], and bacterial biofilms [50–60], as well as mechanically competing tissues [61,62] and spreading epithelia [63–66]. Front stability has also been analyzed when chemotaxis supplements effects like growth and mechanical interactions [37,50,67–69].

Nevertheless, the conditions for the stability of chemotactic fronts remain unknown. Unlike reaction-diffusion systems, which rely only on scalar couplings between fields, chemotaxis couples the population density to the *gradient* of a chemical signal. Thus, the analytical techniques used to study the stability of reaction-diffusion fronts [4] cannot be directly applied to their chemotactic counterparts [70].

*Published by the American Physical Society under the terms of the Creative Commons Attribution 4.0 International license. Further distribution of this work must maintain attribution to the author(s) and the published article's title, journal citation, and DOI. Open access publication funded by the Max Planck Society.*

Here, through direct analysis of their governing equations, we determine the conditions for the linear stability of chemotactic cell fronts. We find that front stability is determined by the ability of cells to sense chemical stimuli at different concentrations, which modulates their response to the chemical gradient and subsequent propagation speeds at different locations along the front. Our calculations reveal two competing mechanisms governing front stability: When cells move ahead of the front, they absorb chemoattractant, causing follower cells to be exposed to (i) a smaller chemical gradient, which slows cells down and promotes stability, and (ii) a lower chemical concentration, which increases the cellular response, speeds cells up, and promotes instability. We predict a chemotactic fingering instability when sensing is limited at low chemical concentrations, for which the tactic response is strong. Therefore, our work links the properties of the sensory machinery of individual cells to the population-scale morphology of chemotactic fronts. Finally, we suggest that this machinery might have evolved to push sensing limitations to high chemical concentrations in order to ensure stable collective chemotaxis.

*Keller-Segel equations.*—Following classic work by Keller and Segel [35,36], we model chemotactic fronts through the coupled dynamics of a chemoattractant (concentration $c$), which has diffusivity $D_c$ and is absorbed by each cell at a maximal rate $k$, and cells (concentration $\rho$), which bias their motion in response to a sensed chemoattractant gradient [Fig. 1(a)]:

$$\partial_t c = D_c \nabla^2 c - k\rho g(c). \tag{1}$$

$$\partial_t \rho = -\boldsymbol{\nabla}\cdot\boldsymbol{J}; \quad \boldsymbol{J} = -D_\rho \boldsymbol{\nabla}\rho + \rho\chi\boldsymbol{\nabla} f(c). \tag{2}$$

Here, $g(c)$ describes how chemoattractant uptake is limited by its availability, modeled using Michaelis-Menten kinetics as $g(c) = c/(c + c_M)$ with half-maximum concentration $c_M$. The cell concentration evolves through the flux $\boldsymbol{J}$, which has a diffusive contribution arising from undirected motion with an effective diffusivity $D_\rho$, and a chemotactic contribution arising from directed motion up the chemical gradient with a drift velocity $\boldsymbol{v}_c = \chi\boldsymbol{\nabla} f(c)$. The function $f(c)$ characterizes the ability of cells to sense the chemoattractant. For illustration purposes, we use the established logarithmic sensing function [17,18,71] $f(c) = \ln\{[1 + c/c_-]/[1 + c/c_+]\}$, with lower and upper characteristic concentrations $c_-$ and $c_+$ [Fig. 1(b), red]. The chemotactic coefficient $\chi$ describes the ability of the cells to migrate up the sensed chemoattractant gradient. In what follows, we determine front stability in terms of $f'(c) > 0$ and $f''(c) < 0$, regardless of the specific form of $f(c)$. Hence, our results can be generalized to other active systems employing different forms of sensing that also typically increase and eventually saturate with increasing stimulus.

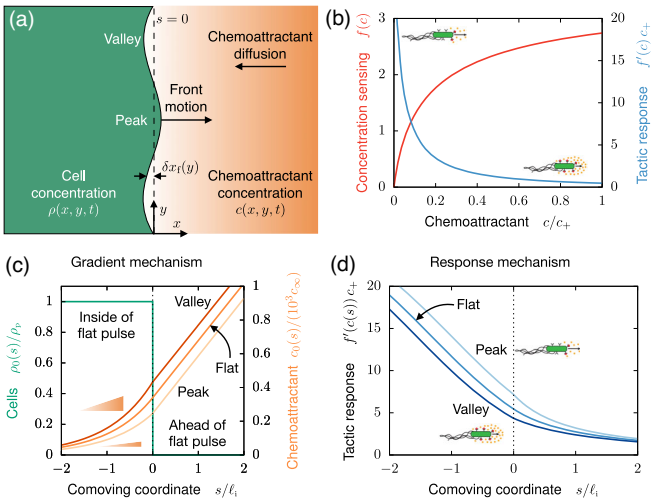


FIG. 1. Competing mechanisms of chemotactic front stability. (a) Schematic of a cell population (green) moving up a chemoattractant gradient (orange). We analyze the stability of a reference flat front (dashed line, located at the origin of the comoving coordinate $s \equiv x - v_0 t = 0$) to perturbations $\delta x_f(y)$, which create peaks and valleys. Note that we did not represent the $y$ dependence of the chemoattractant field. (b) Whereas the ability of cells to sense chemoattractant, $f(c)$, increases with chemoattractant concentration, their tactic response to gradients, $f'(c)$, decreases. (c) Assuming a step profile of cells (green), the chemoattractant profiles for the reference flat front [Eq. (4)] as well as for peaks and valleys of a perturbed front are shown by the orange curves. The comoving coordinate is rescaled by the internal decay length $\ell_i$ (see text). As depicted in the insets, the chemoattractant gradient at $s = 0$ is higher in valleys and lower in peaks, favoring front stability [first term in Eq. (4)]. (d) As depicted in the insets, the cellular response at $s = 0$ is stronger in peaks and weaker in valleys, favoring instability [second term in Eq. (4)]. In (c) and (d) we used front perturbations $\delta x_f(y) = \delta A\ \sin(ky)$ with amplitude $\delta A = 2\ \mu$m and wavelength $\lambda = 2\pi/k = 2$ mm. Parameter values are in Table S1.

While additional details (e.g., other chemicals, cellular proliferation) can also be introduced, here we focus on the minimal model of chemotactic fronts. Indeed, in excellent agreement with experiments, Eqs. (1) and (2) give rise to a propagating pulse of cells [17,18,20,36,38]. However, the full Eqs. (1) and (2) cannot be solved analytically, precluding a generic analysis of front stability.

*Flat front.*—To overcome this issue, we follow earlier work [57] and consider a simplified description of the pulse as a step profile with cell concentration $\rho_p$ moving along the $\hat{\boldsymbol{x}}$ axis at speed $v_0$: $\rho_0(s) = \rho_p\theta(-s)$ [Fig. 1(c), green]. Here, $s \equiv x - v_0 t$ is the comoving coordinate, and $\theta$ is the Heaviside step function. We discuss the validity of this approximation in Supplemental Material [72]. The front of the pulse, located at $s = 0$, is taken to be flat, i.e., independent of the transverse coordinate $y$ [dashed line in Fig. 1(a)]. Ahead of the pulse ($s > 0$), there are no cells, and hence no chemoattractant absorption. Inside the pulse ($s < 0$), chemoattractant is absorbed; we assume that its

concentration is smaller or similar to $c_M$, and hence we approximate $g(c) \approx c/c_M$, whose validity we verify *a posteriori* using our parameter estimates (Table S1). We impose boundary conditions $c(s \to -\infty) = 0$ and $c(s \to \infty) = c_\infty$, with $c_\infty$ being the chemoattractant concentration far ahead of the front, and we require continuity of the chemoattractant concentration and flux at the front.

We thereby obtain the traveling chemoattractant profile $c_0(s)$ [Fig. 1(c), orange]:

$$c_0^a(s) = c_\infty \left[1 - \frac{\sqrt{1+4\Gamma}-1}{\sqrt{1+4\Gamma}+1} \exp\left(-\frac{s}{\ell_d}\right)\right]; \; s \geq 0, \quad (3a)$$

$$c_0^i(s) = \frac{2c_\infty}{\sqrt{1+4\Gamma}+1} \exp\left[\frac{s}{2\ell_d}(\sqrt{1+4\Gamma}-1)\right]; \; s \leq 0. \quad (3b)$$

Ahead of the pulse [Eq. (3a)], the chemoattractant concentration varies exponentially over a diffusion length scale $\ell_d \equiv D_c/v_0$, which results from the balance of front motion and chemoattractant diffusion. Inside the pulse [Eq. (3b)], chemoattractant decays over a different, internal length scale $\ell_i \equiv \sqrt{\ell_d \ell_a} \equiv \ell_d/\sqrt{\Gamma}$, where the absorption length $\ell_a \equiv v_0 c_M/(k\rho_p)$ results from the balance of front motion and chemoattractant absorption. We have also defined the dimensionless parameter $\Gamma \equiv \ell_d/\ell_a$, which we call the diffusio-absorption number. Representative values of all these parameters are given in Table S1.

*Front perturbations.*—We next analyze the linear stability of this front against morphological perturbations. We perturb the cell concentration profile along the $\hat{\boldsymbol{y}}$ axis, transverse to the propagation direction: $\rho(x,y,t) = \rho_0[s - \delta x_f(y,t)]$, where $\delta x_f(y,t)$ represents the perturbation in front position [Fig. 1(a)]. Consequently, the chemoattractant field is perturbed as $c(x,y,t) = c_0(s) + \delta c(s,y,t)$. For perturbations of wave number $q$, the chemoattractant field relaxes at a rate $\sim D_c q^2$ according to Eq. (1). We assume $D_c \gg D_\rho$, as is the case for cells migrating in porous media or on substrates. In this limit, chemoattractant perturbations rapidly reach a quasistationary profile $\delta c(s,y)$ that adapts to the slowly evolving cell front (Supplemental Material [72]).

The cell front moves by diffusion and chemotaxis [Eq. (2)]. As expected, the diffusive flux $-D_\rho \boldsymbol{\nabla}\rho$ tends to stabilize the front by smoothing out transverse gradients of cell concentration. The influence of the chemotactic drift flux $\rho \boldsymbol{v}_c$, however, is more subtle. To gain intuition, we express the chemotactic velocity as $\boldsymbol{v}_c = \chi \boldsymbol{\nabla} f(c) = \chi f'(c) \boldsymbol{\nabla} c$. As in linear response theory, $\boldsymbol{v}_c$ can be viewed as the cellular response to the driving force given by the chemoattractant gradient $\boldsymbol{\nabla} c$ with $\chi f'(c)$ being the response function. Whereas the sensing ability $f(c)$ increases with chemoattractant concentration, the tactic response $f'(c)$ decreases as sensing becomes increasingly saturated [Fig. 1(b)]. Because $\boldsymbol{v}_c$ involves the product of $f'(c)$ and $\boldsymbol{\nabla} c$, its perturbation has two contributions, $\delta \boldsymbol{v}_c = \chi[f'(c)\boldsymbol{\nabla}\delta c + \delta f'(c)\boldsymbol{\nabla} c]$, which correspond to perturbations of the gradient and the response, respectively.

*Competing mechanisms of front stability.*—How do these distinct contributions affect front stability? In a linear stability analysis, to first order in perturbations, front motion depends on the chemotactic velocity perturbation $\delta \boldsymbol{v}_c$ evaluated at the position of the unperturbed front, $s = 0$. While this perturbation has components both in the transverse ($\hat{\boldsymbol{y}}$) and the propagation ($\hat{\boldsymbol{x}}$) directions, as we show in the full analysis in Supplemental Material [72], front stability is determined by the sign of the $\hat{\boldsymbol{x}}$ component,

$$\delta v_{c,x}(s=0,y) = \chi[f_0' \partial_s \delta c(0,y) + \partial_s c_0(0) f_0'' \delta c(0,y)]. \quad (4)$$

Here, we have used $\delta f'(c) = f''(c)\delta c$ and expressed dependencies on $x$ via the comoving coordinate $s = x - v_0 t$; $c_0(s)$ is given by Eq. (3).

The first contribution in Eq. (4) is given by changes in the chemoattractant gradient at the position of the unperturbed front, $\partial_s \delta c(0,y)$, multiplied by the unperturbed chemotactic response, $f_0' \equiv f'[c_0(0)] > 0$. We name this contribution the *gradient mechanism*; it represents changes in cell velocity due to spatial variations in the driving force $\boldsymbol{\nabla} c$. Specifically, in peaks of the perturbed front [$\delta x_f(y) > 0$], cells populate the position of the unperturbed front ($s = 0$), thereby absorbing chemoattractant and decreasing its concentration: $\delta c(0,y) < 0$ [compare peak and flat in Fig. 1(c)]. As a result, the chemoattractant gradient inside the pulse ($s < 0$) decreases with respect to the unperturbed situation [Fig. 1(c)], and thus $\partial_s \delta c(0,y) < 0$. Because this first contribution in Eq. (4) is negative, it is stabilizing. Intuitively, the decrease in chemoattractant gradient slows down cells in peaks, allowing the rest of the population to catch up and flatten the front.

The second contribution in Eq. (4) is given by the unperturbed chemoattractant gradient, $\partial_s c_0(0) > 0$, multiplied by the change in the chemotactic response at the front, $\delta f'(c) = f_0'' \delta c$, where $f_0'' \equiv f''(c_0(0)) < 0$ [Fig. 1(b)]. We name this contribution the *response mechanism*; it represents changes in cell velocity due to spatial variations in the cells' chemotactic response. As noted above, in peaks of the perturbed front [$\delta x_f(y) > 0$], cells absorb chemoattractant and decrease its concentration at $s = 0$, giving $\delta c(0,y) < 0$. Because this second contribution in Eq. (4) is positive, it is destabilizing. Intuitively, the decrease in chemoattractant causes cells in peaks to respond to the gradient more strongly [compare peak and flat in Fig. 1(d)] and move faster, leaving the rest of the population behind and amplifying front perturbations.

Thus, our analysis reveals two competing chemotactic mechanisms that determine front stability: Cells at a bulging part of the front are exposed to a smaller chemoattractant gradient, which slows them down (gradient mechanism), but they respond more strongly to the gradient, which speeds them up (response mechanism).

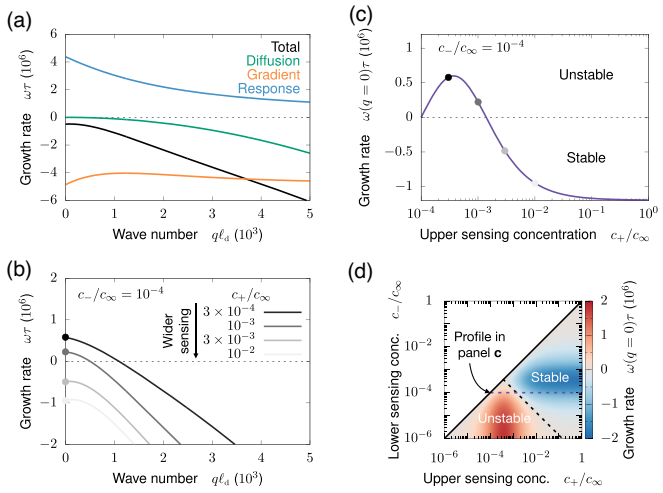


FIG. 2. Cellular sensing governs chemotactic front stability. (a) Growth rate of front perturbations, showing the contributions of cell diffusion as well as the gradient and response chemotactic mechanisms [see Figs. 1(c) and 1(d)]. (b) Increasing the upper sensing concentration $c_+$ promotes front stability. (c) As sensing becomes less limited at higher concentrations by increasing $c_+$, the front can switch from unstable to stable, as indicated by the sign of the long-wavelength growth rate $\omega(q=0)$. The points correspond to those in panel (b). (d) Diagram of front stability as a function of the lower and upper characteristic sensing concentrations. The color code informs about the degree of front stability, as given by $\omega(q=0)$. The black dashed line indicates the stability limit [Eq. (7)]. The purple dashed line indicates the slice of the diagram shown in panel (c). Throughout the figure, the growth rate is rescaled by what we call the chemotactic time $\tau \equiv \ell_d^2/\chi$. Parameter values are in Table S1.

To quantitatively compare these two mechanisms, we rewrite Eq. (4) as $\delta v_{c,x}(s=0,y) = \chi[\alpha\partial_s - \beta c_0'(0)/c_\infty]\,\delta c(0,y)/c_\infty$, where the two positive dimensionless parameters $\alpha \equiv f_0' c_\infty$ and $\beta \equiv -f_0'' c_\infty^2$ quantify the strengths of the gradient and response mechanisms, respectively.

*Chemotactic fingering instability.*—Having identified the two mechanisms whereby chemotaxis influences front stability, we solve the full Eq. (2) to obtain front speed perturbations $\delta v(y,t) = \partial_t \delta x_f(y,t)$ [Eq. (S14)], and hence the growth rate $\omega(q) \equiv \delta\tilde{v}(q)/\delta\tilde{x}_f(q)$ of front perturbations with wave number $q$, where tildes indicate Fourier components (Supplemental Material [72]):

$$\omega(q) = -D_\rho q^2 + \frac{\chi}{\ell_d^2}\frac{\sqrt{1+4\Gamma}-1}{\sqrt{1+4q^2\ell_d^2}+\sqrt{1+4(\Gamma+q^2\ell_d^2)}} \times\left[\beta\frac{\sqrt{1+4\Gamma}-1}{\sqrt{1+4\Gamma}+1} - \frac{\alpha}{2}\left(\sqrt{1+4(\Gamma+q^2\ell_d^2)}-1\right) -2\alpha\frac{q^2\ell_d^2}{\sqrt{1+4(\Gamma+q^2\ell_d^2)}-1}\right]. \tag{5}$$

Figure 2(a) shows this growth rate separating the contributions of the different mechanisms. As expected, the diffusive contribution $-D_\rho q^2$ is always stabilizing [Fig. 2(a), green]. At large length scales (small $q$), it is negligible in front of the two chemotactic mechanisms resulting from Eq. (4). In agreement with our argument above, the *gradient mechanism* [$\propto \alpha$ in Eq. (5)] is stabilizing [Fig. 2(a), orange], while the *response mechanism* [$\propto \beta$ in Eq. (5)] is destabilizing [Fig. 2(a), blue]. In the long-wavelength limit ($q \to 0$), we have $\omega(0) = (\chi/\ell_d^2)\,[(\sqrt{1+4\Gamma}-1)/(\sqrt{1+4\Gamma}+1)]^2[\beta - (\alpha/2)(\sqrt{1+4\Gamma}+1)]$, and hence the flat front becomes unstable, $\omega(0) > 0$, if

$$\beta > \frac{\alpha}{2}(\sqrt{1+4\Gamma}+1), \tag{6}$$

i.e., if the chemotactic response decreases too strongly with chemoattractant concentration, corresponding to large values of $\beta$. In this case, cells at valleys, which are exposed to higher concentrations, respond too weakly and are left behind by cells at peaks, which are instead exposed to lower concentrations and thus respond more strongly to the gradient.

*Cellular sensing governs chemotactic front stability.*—Our central result, given by Eqs. (5) and (6), is that the limited ability of single cells to sense high concentrations of chemoattractant, and the resulting limitation in their chemotactic response, can destabilize entire propagating fronts. To illustrate this, we recast our results in terms of the characteristic concentrations $c_-$ and $c_+$ of the sensing function $f(c)$. Varying these concentrations tunes both $f'(c)$ and $f''(c)$, thus affecting the values of both $\alpha \equiv f_0' c_\infty$ and $\beta \equiv -f_0'' c_\infty^2$, and hence changing the relative contribution of the stabilizing and the destabilizing mechanisms. Which effect wins when varying $c_-$ and $c_+$?

For a given $c_-$, the front is unstable for values of $c_+$ close to $c_-$, i.e., for narrow sensing windows [darker curves in Fig. 2(b)]. As $c_+$ increases, the destabilizing effect of the chemotactic response limitation becomes less important, and the front eventually becomes stable [lighter curves in Fig. 2(b)]. Therefore, for a given $c_-$, the front switches from unstable to stable as the sensing window widens by increasing $c_+$ [Fig. 2(c), corresponding to the purple dashed line in Fig. 2(d)]. Conversely, the front can also be stabilized by narrowing the sensing window, e.g., by increasing $c_-$ at fixed $c_+$ [moving up in Fig. 2(d)]. Therefore, front stability is promoted by increasing the characteristic sensing concentrations $c_-$ and $c_+$. Although increasing $c_-$ and $c_+$ weakens the chemotactic response [Fig. 1(b)], it also makes the destabilizing response-limitation effects less pronounced. Finally, we recast the instability condition, Eq. (6), in terms of $c_-$ and $c_+$:

$$\frac{c_+}{c_\infty} < \frac{c_\infty}{c_-}\frac{2}{1+2\Gamma+\sqrt{1+4\Gamma}}. \tag{7}$$

The black dashed line in Fig. 2(d) shows the stability limit.

To test our predictions, we perform finite-element simulations of the full Eqs. (1) and (2) (Supplemental Material [72]). Introducing an initial perturbation with a long wavelength ($q\ell_d = 0.02$) and small amplitude ($A/\lambda = 0.016$), we find regimes of both front instability and stability (Fig. S1) in agreement with the stability diagram predicted analytically (Fig. S2).

*Discussion.*—We have quantified the conditions for the stability of chemotactic fronts. Below the stability limit [Eq. (7)], we predict a morphological instability that could result in fingering patterns and even front disassembly. Expanding bacterial colonies form complex patterns that are thought to arise from bulk instabilities [12,15,16,37,73,74]. However, the instability that we predict is fundamentally different, as it is interfacial and it arises purely from chemotaxis. To our knowledge, it has not been observed in experiments. Our predictions provide guidelines for future studies to search for it. For example, we predict front instability when the sensing concentrations $c_-$ and $c_+$ are small compared to nutrient availability $c_\infty$ [Fig. 2(d)]. Therefore, experiments can probe this regime by either increasing nutrient availability or genetically impairing the cells' sensing ability. Moreover, we predict that fronts would destabilize over long wavelengths, at least of the order of the diffusion length $\ell_d$ [Fig. 2(b)]. In experiments, fronts must therefore be sufficiently long to become unstable.

Front stability can have relevant biological implications. For example, in embryos, chemotactic cell groups must remain cohesive to develop into functional organs. In bacterial populations, cells must also stay together to collectively absorb sufficient chemoattractant to generate the chemical gradient driving front motion [75,76]. Thus, inspired by our calculations, we speculate that the cells' sensing abilities might have evolved to avoid instability and ensure robust collective chemotaxis.

To probe this idea, we examine published experiments on chemotactic fronts of *E. coli* [17,20]. These experiments report the concentrations $c_-$ and $c_+$ for two different chemoattractants, as well as the parameters that determine the diffusio-absorption number $\Gamma$ (Table S2), with which we construct a stability diagram akin to Fig. 2(d) for each experiment (Fig. S4). The far-field concentrations $c_\infty$ used in experiments likely represent upper bounds of those encountered in natural environments, and thus our estimates are in conditions most favorable for *instability*. Yet, we find that all experiments fall in the predicted *stable* regime. Consistently, the experiments observe stable flat fronts in all cases, suggesting that the ratios $c_-/c_\infty$ and $c_+/c_\infty$ are always high enough (Fig. S4). Further experiments are required to systematically test the tantalizing hypothesis that cellular sensing might be tuned to ensure stable collective chemotaxis.

Our results are also qualitatively consistent with recent experiments on 3D-printed bacterial populations, which found that morphological perturbations are smoothed out by chemotaxis [77]. These experiments, however, imposed large-amplitude perturbations in three-dimensional populations, whereas our analysis focuses on the small-amplitude limit in two dimensions. Hence, the experiments cannot be directly compared to our theory. Nevertheless, both demonstrate that sensing limitations of individual cells determine the stability of an entire chemotactic population.

Building on this finding, future work can explore how population morphology is affected by the chemotactic efficiency constraints imposed by biochemical [78–81] and mechanical [82,83] cell-cell interactions, switching between swimming states [84], and information acquisition requirements [85]. Our work could also be generalized to account for collective sensing mechanisms [78] and for chemokinesis, i.e., the dependence of cell speed on chemical concentration [86]. Furthermore, whereas the instability mechanisms that we identified arise from the deterministic dynamics of chemotaxis, future work can study the role of noise in selecting the resulting patterns. Beyond chemotaxis, our theory could be generalized to other types of collective tactic phenomena [87–89] including cell durotaxis [90,91], electrotaxis [92], and robot phototaxis [93,94]. In these cases, as for chemotaxis, sensing increases and then saturates with the stimulus, be it substrate stiffness [91,95], electric field [92], or light intensity [93,94]—which, as quantified by the sensing function $f(c)$, is the essential feature of our theory. Specifically, in our analysis of chemotactic front propagation in terms of linear response theory, chemical gradients provide the driving force, and cellular sensing provides the response function. In these general terms, we conclude that, when modulated by a response function, the force that drives front propagation can also fully determine its stability.

We thank D. B. Amchin, T. Bhattacharjee, and N. S. Wingreen for useful discussions. R. A. acknowledges support from the Princeton Center for Theoretical Science, from the Human Frontier Science Program (LT000475/2018-C), and from the National Science Foundation through the Center for the Physics of Biological Function (PHY-1734030). A. M.-C. acknowledges support from the Princeton Center for Theoretical Science and the Human Frontier Science Program through Grant No. LT000035/2021-C. S. S. D. acknowledges support from NSF Grant No. CBET-1941716, the Eric and Wendy Schmidt Transformative Technology Fund at Princeton, the Princeton Center for Complex Materials, a Materials Research Science and Engineering Center supported by NSF Grant No. DMR-2011750, and the Pew Biomedical Scholars program.

*ricard.alert@princeton.edu
†ssdatta@princeton.edu

[1] M. Cross and P. Hohenberg, Pattern formation outside of equilibrium, Rev. Mod. Phys. **65**, 851 (1993).

[2] Michael Cross and Henry Greenside, *Pattern Formation and Dynamics in Nonequilibrium Systems* (Cambridge University Press, Cambridge, England, 2009).

[3] L. M. Pismen, *Patterns and Interfaces in Dissipative Dynamics* (Springer, New York, 2006).

[4] Rashmi C. Desai and Raymond Kapral, *Dynamics of Self-Organized and Self-Assembled Structures* (Cambridge University Press, Cambridge, England, 2009).

[5] Wim van Saarloos, Front propagation into unstable states, Phys. Rep. **386**, 29 (2003).

[6] *Pattern Formation at Interfaces*, edited by Pierre Colinet and Alexander Nepomnyashchy (Springer, New York, 2010).

[7] James Dickson Murray, *Mathematical Biology I. An Introduction*, 3rd ed. (Springer, New York, 2002).

[8] Leah Edelstein-Keshet, *Mathematical Models in Biology* (Society for Industrial and Applied Mathematics, Philadelphia, 2005).

[9] Jose Negrete and Andrew C. Oates, Towards a physical understanding of developmental patterning, Nat. Rev. Genet. **22**, 518 (2021).

[10] R. A. Fisher, The wave of advance of advantageous genes, Ann. Eugen. **7**, 355 (1937).

[11] A. N. Kolmogorov, I. G. Petrovsky, and N. S. Piskunov, A study of the diffusion equation with increase in the amount of substance, and its application to a biological problem, Bull. Moscow Univ. Math. Mech. **1**, 1 (1937).

[12] James Dickson Murray, *Mathematical Biology II. Spatial Models and Biomedical Applications*, 3rd ed. (Springer, New York, 2003).

[13] Remy Colin, Bin Ni, Leanid Laganenka, and Victor Sourjik, Multiple functions of flagellar motility and chemotaxis in bacterial physiology, FEMS Microbiol. Rev. **45**, fuab038 (2021).

[14] J. Adler, Chemotaxis in Bacteria, Science **153**, 708 (1966).

[15] Elena O. Budrene and Howard C. Berg, Complex patterns formed by motile cells of Escherichia coli, Nature (London) **349**, 630 (1991).

[16] Elena O. Budrene and Howard C. Berg, Dynamics of formation of symmetrical patterns by chemotactic bacteria, Nature (London) **376**, 49 (1995).

[17] X. Fu, S. Kato, J. Long, H. H. Mattingly, C. He, D. C. Vural, S. W. Zucker, and T. Emonet, Spatial self-organization resolves conflicts between individuality and collective migration, Nat. Commun. **9**, 2177 (2018).

[18] Jonas Cremer, Tomoya Honda, Ying Tang, Jerome Wong-Ng, Massimo Vergassola, and Terence Hwa, Chemotaxis as a navigation strategy to boost range expansion, Nature (London) **575**, 658 (2019).

[19] Sebastian Gude, Erçağ Pinçe, Katja M. Taute, Anne-Bart Seinen, Thomas S. Shimizu, and Sander J. Tans, Bacterial coexistence driven by motility and spatial competition, Nature (London) **578**, 588 (2020).

[20] Tapomoy Bhattacharjee, Daniel B. Amchin, Jenna A. Ott, Felix Kratz, and Sujit S. Datta, Chemotactic migration of bacteria in porous media, Biophys. J. **120**, 3483 (2021).

[21] Yang Bai, Caiyun He, Pan Chu, Junjiajia Long, Xuefei Li, and Xiongfei Fu, Spatial modulation of individual behaviors enables an ordered structure of diverse phenotypes during bacterial group migration, eLife **10**, e67316 (2021).

[22] Evelyn F. Keller and Lee A. Segel, Initiation of slime mold aggregation viewed as an instability, J. Theor. Biol. **26**, 399 (1970).

[23] Elena Scarpa and Roberto Mayor, Collective cell migration in development, J. Cell Biol. **212**, 143 (2016).

[24] K. J. Painter, P. K. Maini, and H. G. Othmer, Stripe formation in juvenile Pomacanthus explained by a generalized Turing mechanism with chemotaxis, Proc. Natl. Acad. Sci. U.S.A. **96**, 5549 (1999).

[25] Eric Theveneau, Lorena Marchant, Sei Kuriyama, Mazhar Gull, Barbara Moepps, Maddy Parsons, and Roberto Mayor, Collective chemotaxis requires contact-dependent cell polarity, Dev. Cell **19**, 39 (2010).

[26] Luke Tweedy, Peter A. Thomason, Peggy I. Paschke, Kirsty Martin, Laura M. Machesky, Michele Zagnoni, and Robert H. Insall, Seeing around corners: Cells solve mazes and respond at a distance using attractant breakdown, Science **369**, eaay9792 (2020).

[27] Gema Malet-Engra, Weimiao Yu, Amanda Oldani, Javier Rey-Barroso, Nir S Gov, Giorgio Scita, and Loïc Dupré, Collective cell motility promotes chemotactic prowess and resistance to chemorepulsion, Curr. Biol. **25**, 242 (2015).

[28] Alberto Puliafito, Alessandro De Simone, Giorgio Seano, Paolo Armando Gagliardi, Laura Di Blasio, Federica Chianale, Andrea Gamba, Luca Primo, and Antonio Celani, Three-dimensional chemotaxis-driven aggregation of tumor cells, Sci. Rep. **5**, 15205 (2015).

[29] Ah-Young Jee, Sandipan Dutta, Yoon-Kyoung Cho, Tsvi Tlusty, and Steve Granick, Enzyme leaps fuel antichemotaxis, Proc. Natl. Acad. Sci. U.S.A. **115**, 14 (2018).

[30] Jaime Agudo-Canalejo, Pierre Illien, and Ramin Golestanian, Phoresis and enhanced diffusion compete in enzyme chemotaxis, Nano Lett. **18**, 2711 (2018).

[31] Farzad Mohajerani, Xi Zhao, Ambika Somasundar, Darrell Velegol, and Ayusman Sen, A theory of enzyme chemotaxis: From experiments to modeling, Biochemistry **57**, 6256 (2018).

[32] Pierre Illien, Ramin Golestanian, and Ayusman Sen, "Fuelled" motion: Phoretic motility and collective behaviour of active colloids, Chem. Soc. Rev. **46**, 5508 (2017).

[33] Benno Liebchen and Hartmut Löwen, Synthetic chemotaxis and collective behavior in active matter, Acc. Chem. Res. **51**, 2982 (2018).

[34] Holger Stark, Artificial chemotaxis of self-phoretic active colloids: Collective behavior, Acc. Chem. Res. **51**, 2681 (2018).

[35] Evelyn F. Keller and Lee A. Segel, Model for chemotaxis, J. Theor. Biol. **30**, 225 (1971).

[36] Evelyn F. Keller and Lee A. Segel, Traveling bands of chemotactic bacteria: A theoretical analysis, J. Theor. Biol. **30**, 235 (1971).

[37] M. P. Brenner, L. S. Levitov, and E. O. Budrene, Physical mechanisms for chemotactic pattern formation by bacteria, Biophys. J. **74**, 1677 (1998).

[38] Maximilian Seyrich, Andrzej Palugniok, and Holger Stark, Traveling concentration pulses of bacteria in a generalized Keller–Segel model, New J. Phys. **21**, 103001 (2019).

[39] Avaneesh V. Narla, Jonas Cremer, and Terence Hwa, A traveling-wave solution for bacterial chemotaxis with growth, Proc. Natl. Acad. Sci. U.S.A. **118**, e2105138118 (2021).

[40] J. P. Gollub and J. S. Langer, Pattern formation in nonequilibrium physics, Rev. Mod. Phys. **71**, S396 (1999).
[41] R. Gonzalez-Cinca, R. Folch, R. Benitez, L. Ramirez-Piscina, J. Casademunt, and A. Hernandez-Machado, *Phase-field models in interfacial pattern formation out of equilibrium, in Advances in Condensed Matter and Statistical Mechanics*, edited by Elka Korutcheva and Rodolfo Cuerno (Nova Science Publishers, New York, 2004), Chap. 9, pp. 203–236.
[42] Jaume Casademunt, Viscous fingering as a paradigm of interfacial pattern formation: Recent results and new challenges, Chaos **14**, 809 (2004).
[43] J. S. Langer, Instabilities and pattern formation in crystal growth, Rev. Mod. Phys. **52**, 1 (1980).
[44] Eshel Ben-Jacob and Peter Garik, The formation of patterns in non-equilibrium growth, Nature (London) **343**, 523 (1990).
[45] P. G. Saffman and G. Taylor, The penetration of a fluid into a porous medium or Hele-Shaw cell containing a more viscous liquid, Proc. R. Soc. A **245**, 312 (1958).
[46] W. W. Mullins and R. F. Sekerka, Stability of a planar interface during solidification of a dilute binary alloy, J. Appl. Phys. **35**, 444 (1964).
[47] Michelle Driscoll, Blaise Delmotte, Mena Youssef, Stefano Sacanna, Aleksandar Donev, and Paul Chaikin, Unstable fronts and motile structures formed by microrollers, Nat. Phys. **13**, 375 (2017).
[48] Evgeniy Khain and Leonard M. Sander, Dynamics and Pattern Formation in Invasive Tumor Growth, Phys. Rev. Lett. **96**, 188103 (2006).
[49] Michał Bogdan and Thierry Savin, Fingering instabilities in tissue invasion: An active fluid model, R. Soc. Open Sci. **5**, 181579 (2018).
[50] Eshel Ben-Jacob, Inon Cohen, and Herbert Levine, Cooperative self-organization of microorganisms, Adv. Phys. **49**, 395 (2000).
[51] Rosalind J. Allen and Bartlomiej Waclaw, Bacterial growth: A statistical physicist's guide, Rep. Prog. Phys. **82**, 016601 (2019).
[52] Romain Mueller and Amin Doostmohammadi, Phase field models of active matter, arXiv:2102.05557.
[53] So Kitsunezaki, Interface dynamics for bacterial colony formation, J. Phys. Soc. Jpn. **66**, 1544 (1997).
[54] Judith Müller and Wim van Saarloos, Morphological instability and dynamics of fronts in bacterial growth models with nonlinear diffusion, Phys. Rev. E **65**, 061111 (2002).
[55] F. D. C. Farrell, O. Hallatschek, D. Marenduzzo, and B. Waclaw, Mechanically Driven Growth of Quasi-Two-Dimensional Microbial Colonies, Phys. Rev. Lett. **111**, 168101 (2013).
[56] Amin Doostmohammadi, Sumesh P. Thampi, and Julia M. Yeomans, Defect-Mediated Morphologies in Growing Cell Colonies, Phys. Rev. Lett. **117**, 048102 (2016).
[57] Xin Wang, Howard A. Stone, and Ramin Golestanian, Shape of the growing front of biofilms, New J. Phys. **19**, 125007 (2017).
[58] Sarah Trinschek, Karin John, and Uwe Thiele, Modelling of surfactant-driven front instabilities in spreading bacterial colonies, Soft Matter **14**, 4464 (2018).
[59] Jing Yan, Chenyi Fei, Sheng Mao, Alexis Moreau, Ned S. Wingreen, Andrej Košmrlj, Howard A. Stone, and Bonnie L. Bassler, Mechanical instability and interfacial energy drive biofilm morphogenesis, eLife **8**, e43920 (2019).
[60] Chenyi Fei, Sheng Mao, Jing Yan, Ricard Alert, Howard A. Stone, Bonnie L. Bassler, Ned S. Wingreen, and Andrej Košmrlj, Nonuniform growth and surface friction determine bacterial biofilm morphology on soft substrates, Proc. Natl. Acad. Sci. U.S.A. **117**, 7622 (2020).
[61] John J. Williamson and Guillaume Salbreux, Stability and Roughness of Interfaces in Mechanically Regulated Tissues, Phys. Rev. Lett. **121**, 238102 (2018).
[62] Tobias Büscher, Angel L. Diez, Gerhard Gompper, and Jens Elgeti, Instability and fingering of interfaces in growing tissue, New J. Phys. **22**, 083005 (2020).
[63] Ricard Alert and Xavier Trepat, Physical models of collective cell migration, Annu. Rev. Condens. Matter Phys. **11**, 77 (2020).
[64] Carlos Pérez-González, Ricard Alert, Carles Blanch-Mercader, Manuel Gómez-González, Tomasz Kolodziej, Elsa Bazellieres, Jaume Casademunt, and Xavier Trepat, Active wetting of epithelial tissues, Nat. Phys. **15**, 79 (2019).
[65] Ricard Alert, Carles Blanch-Mercader, and Jaume Casademunt, Active Fingering Instability in Tissue Spreading, Phys. Rev. Lett. **122**, 088104 (2019).
[66] Carolina Trenado, Luis L. Bonilla, and Alejandro Martínez-Calvo, Fingering instability in spreading epithelial monolayers: Roles of cell polarisation, substrate friction and contractile stresses, Soft Matter **17**, 8276 (2021).
[67] Eshel Ben-Jacob, Ofer Schochet, Adam Tenenbaum, Inon Cohen, Andras Czirók, and Tamas Vicsek, Generic modelling of cooperative growth patterns in bacterial colonies, Nature (London) **368**, 46 (1994).
[68] Martine Ben Amar, Chemotaxis migration and morphogenesis of living colonies, Eur. Phys. J. E **36**, 64 (2013).
[69] M. Ben Amar, Collective chemotaxis and segregation of active bacterial colonies, Sci. Rep. **6**, 21269 (2016).
[70] Mitsuo Funaki, Masayasu Mimura, and Tohru Tsujikawa, Travelling front solutions arising in the chemotaxis-growth model, Interfaces Free Boundaries **8**, 223 (2006).
[71] Yevgeniy V. Kalinin, Lili Jiang, Yuhai Tu, and Mingming Wu, Logarithmic sensing in Escherichia coli bacterial chemotaxis, Biophys. J. **96**, 2439 (2009).
[72] See Supplemental Material at http://link.aps.org/supplemental/10.1103/PhysRevLett.128.148101 for discussion of the step-profile approximation, details of the linear stability analysis, numerical solutions, and analysis of experiments.
[73] M. E. Cates, D. Marenduzzo, I. Pagonabarraga, and J. Tailleur, Arrested phase separation in reproducing bacteria creates a generic route to pattern formation, Proc. Natl. Acad. Sci. U.S.A. **107**, 11715 (2010).
[74] Michael P. Brenner, Chemotactic patterns without chemotaxis, Proc. Natl. Acad. Sci. U.S.A. **107**, 11653 (2010).
[75] Luke Tweedy, Olivia Susanto, and Robert H. Insall, Self-generated chemotactic gradients—cells steering themselves, Curr. Opin. Cell Biol. **42**, 46 (2016).
[76] Luke Tweedy and Robert H. Insall, Self-generated gradients yield exceptionally robust steering cues, Front. Cell Dev. Biol. **8**, 133 (2020).

[77] Tapomoy Bhattacharjee, Daniel B. Amchin, Ricard Alert, J. A. Ott, and Sujit S. Datta, Chemotactic smoothing of collective migration, eLife **11**, e71226 (2022).
[78] Brian A. Camley, Collective gradient sensing and chemotaxis: Modeling and recent developments, J. Phys. Condens. Matter **30**, 223001 (2018).
[79] David Ellison, Andrew Mugler, Matthew D Brennan, Sung Hoon Lee, Robert J. Huebner, Eliah R. Shamir, Laura A. Woo, Joseph Kim, Patrick Amar, Ilya Nemenman, Andrew J. Ewald, and Andre Levchenko, Cell-cell communication enhances the capacity of cell ensembles to sense shallow gradients during morphogenesis, Proc. Natl. Acad. Sci. U.S.A. **113**, E679 (2016).
[80] Andrew Mugler, Andre Levchenko, and Ilya Nemenman, Limits to the precision of gradient sensing with spatial communication and temporal integration, Proc. Natl. Acad. Sci. U.S.A. **113**, E689 (2016).
[81] Sean Fancher and Andrew Mugler, Fundamental Limits to Collective Concentration Sensing in Cell Populations, Phys. Rev. Lett. **118**, 078101 (2017).
[82] Remy Colin, Knut Drescher, and Victor Sourjik, Chemotactic behaviour of Escherichia coli at high cell density, Nat. Commun. **10**, 5329 (2019).
[83] Maojin Tian, Chi Zhang, Rongjing Zhang, and Junhua Yuan, Collective motion enhances chemotaxis in a two-dimensional bacterial swarm, Biophys. J. **120**, 1615 (2021).
[84] Zahra Alirezaeizanjani, Robert Großmann, Veronika Pfeifer, Marius Hintsche, and Carsten Beta, Chemotaxis strategies of bacteria with multiple run modes, Sci. Adv. **6**, eaaz6153 (2020).
[85] H. H. Mattingly, K. Kamino, B. B. Machta, and T. Emonet, *Escherichia coli* chemotaxis is information limited, Nat. Phys. **17**, 1426 (2021).
[86] Theresa Jakuszeit, James Lindsey-Jones, François J. Peaudecerf, and Ottavio A. Croze, Migration and accumulation of bacteria with chemotaxis and chemokinesis, Eur. Phys. J. E **44**, 32 (2021).
[87] Pere Roca-Cusachs, Raimon Sunyer, and Xavier Trepat, Mechanical guidance of cell migration: Lessons from chemotaxis, Curr. Opin. Cell Biol. **25**, 543 (2013).
[88] Adam Shellard and Roberto Mayor, All roads lead to directional cell migration, Trends Cell Biol. **30**, 852 (2020).
[89] Shuvasree SenGupta, Carole A. Parent, and James E. Bear, The principles of directed cell migration, Nat. Rev. Mol. Cell Biol. **22**, 529 (2021).
[90] Raimon Sunyer, Vito Conte, Jorge Escribano, Alberto Elosegui-Artola, Anna Labernadie, Léo Valon, Daniel Navajas, José Manuel García-Aznar, José J. Muñoz, Pere Roca-Cusachs, and Xavier Trepat, Collective cell durotaxis emerges from long-range intercellular force transmission, Science **353**, 1157 (2016).
[91] Ricard Alert and Jaume Casademunt, Role of substrate stiffness in tissue spreading: Wetting transition and tissue durotaxis, Langmuir **35**, 7571 (2019).
[92] Daniel J. Cohen, W. James Nelson, and Michel M Maharbiz, Galvanotactic control of collective cell migration in epithelial monolayers, Nat. Mater. **13**, 409 (2014).
[93] Mite Mijalkov, Austin McDaniel, Jan Wehr, and Giovanni Volpe, Engineering Sensorial Delay to Control Phototaxis and Emergent Collective Behaviors, Phys. Rev. X **6**, 011008 (2016).
[94] Stefano Palagi and Peer Fischer, Bioinspired microrobots, Nat. Rev. Mater. **3**, 113 (2018).
[95] Marion Ghibaudo, Alexandre Saez, Léa Trichet, Alain Xayaphoummine, Julien Browaeys, Pascal Silberzan, Axel Buguin, and Benoît Ladoux, Traction forces and rigidity sensing regulate cell functions, Soft Matter **4**, 1836 (2008).